2-1-2024

# Optimal approaches to analyzing functional MRI data in glioma patients

Ki Yun Park
*Washington University School of Medicine in St. Louis*
Joshua S Shimony
*Washington University School of Medicine in St. Louis*
Satrajit Chakrabarty
*Washington University in St. Louis*
Aaron B Tanenbaum
*Washington University School of Medicine in St. Louis*
Carl D Hacker
*Washington University School of Medicine in St. Louis*

*See next page for additional authors*

Journal of Neuroscience Methods 402 (2024) 110011

Contents lists available at ScienceDirect

Journal of Neuroscience Methods

journal homepage: www.elsevier.com/locate/jneumeth

# Optimal approaches to analyzing functional MRI data in glioma patients

Ki Yun Park [a,b,k,*], Joshua S. Shimony [c], Satrajit Chakrabarty [i], Aaron B. Tanenbaum [d], Carl D. Hacker [a], Kara M. Donovan [e,k], Patrick H. Luckett [a,k], Mikhail Milchenko [c], Aristeidis Sotiras [c,j], Daniel S. Marcus [c], Eric C. Leuthardt [a,e,f,g,h,k], Abraham Z. Snyder [c,d]

[a] Department of Neurological Surgery, Washington University School of Medicine, St. Louis, MO 63110, USA
[b] Medical Scientist Training Program, Washington University School of Medicine, St. Louis, MO, USA
[c] Mallinckrodt Institute of Radiology, Washington University School of Medicine, St. Louis, MO 63110, USA
[d] Department of Neurology, Washington University School of Medicine, St. Louis, MO 63110, USA
[e] Department of Biomedical Engineering, Washington University, St. Louis, MO 63130, USA
[f] Department of Mechanical Engineering and Materials Science, Washington University, St. Louis, MO 63130, USA
[g] Center for Innovation in Neuroscience and Technology, Washington University School of Medicine, St. Louis, MO 63110, USA
[h] Brain Laser Center, Washington University School of Medicine, St. Louis, MO 63110, USA
[i] Department of Electrical and Systems Engineering, Washington University, St. Louis, MO 63130, USA
[j] Institute for Informatics, Data Science & Biostatistics, Washington University School of Medicine, St. Louis, MO 63110, USA
[k] Division of Neurotechnology, Washington University School of Medicine, St. Louis, MO 63110, USA

ARTICLE INFO

*Keywords:*
Glioma
Resting-state fMRI
Atlas registration
Parcellation schemes
Parcellation granularity
Graph-theoretic measures

ABSTRACT

*Background:* Resting-state fMRI is increasingly used to study the effects of gliomas on the functional organization of the brain. A variety of preprocessing techniques and functional connectivity analyses are represented in the literature. However, there so far has been no systematic comparison of how alternative methods impact observed results.

*New method:* We first surveyed current literature and identified alternative analytical approaches commonly used in the field. Following, we systematically compared alternative approaches to atlas registration, parcellation scheme, and choice of graph-theoretical measure as regards differentiating glioma patients (N = 59) from age-matched reference subjects (N = 163).

*Results:* Our results suggest that non-linear, as opposed to affine registration, improves structural match to an atlas, as well as measures of functional connectivity. Functionally- as opposed to anatomically-derived parcellation schemes maximized the contrast between glioma patients and reference subjects. We also demonstrate that graph-theoretic measures strongly depend on parcellation granularity, parcellation scheme, and graph density.

*Comparison with existing methods and conclusions:* Our current work primarily focuses on technical optimization of rs-fMRI analysis in glioma patients and, therefore, is fundamentally different from the bulk of papers discussing glioma-induced functional network changes. We report that the evaluation of glioma-induced alterations in the functional connectome strongly depends on analytical approaches including atlas registration, choice of parcellation scheme, and graph-theoretical measures.

*Abbreviations:* AAL, Automated Anatomical Labelling; AFF, 12-parameter affine registration with no masking; ANTs, The Advanced Normalization Tools diffeomorphic algorithm (https://www.nitrc.org/projects/ants); BOLD, Blood-Oxygenated-Level-Dependent; CFM, Cost-function masking; DVARS, D refers to temporal derivative of timeseries; VARS refer to RMS, variance over voxels; FC, Functional Connectivity; FWHM, full width at half maximum; NL+M, Non-linear registration with cost function masking; NL-M, Non-linear registration with no masking; OASIS3, Open Access Series of Imaging Studies; rs-fMRI, Resting-state functional Magnetic Resonance Imaging; RSNs, Resting State Networks.

* Correspondence to: Department of Neurological Surgery, Washington University in St. Louis, USA.
*E-mail address:* k.park@wustl.edu (K.Y. Park).

https://doi.org/10.1016/j.jneumeth.2023.110011
Received 17 August 2023; Received in revised form 18 September 2023; Accepted 9 November 2023
Available online 18 November 2023

## 1. Introduction

Functional magnetic resonance imaging (fMRI) is increasingly used to study patients with gliomas (Lv et al., 2022; Sighinolfi et al., 2022). Analysis of resting state fMRI (rs-fMRI) data involves evaluation of statistical features of spontaneous fluctuations in blood-oxygenated-level-dependent (BOLD) signals observed in the task-free state. Spontaneous fluctuations of BOLD signals are correlated over widely distributed regions of the brain. This phenomenon is referred to as functional connectivity (FC). The associated topographies are known as resting state networks (RSNs) (Beckmann et al., 2005) or intrinsic connectivity networks (Seeley et al., 2007).

The primary applications of rs-fMRI in glioma patients are presurgical functional mapping (Dierker et al., 2017; Leuthardt et al., 2018; Park et al., 2020) and the study of tumor-induced functional reorganization of the brain (Daniel et al., 2021; Fox and King, 2018; Ghinda et al., 2018). Although task-based fMRI has frequently been used in this context, rs-fMRI offers the advantage that it does not rely on patient compliance with a task paradigm. Further, a rich array of analysis strategies can be applied to rs-fMRI data (Hacker et al., 2013; Zang et al., 2007; Zou et al., 2008). Although much has been learned from prior work, e.g., (Fox and King, 2018; Ghinda et al., 2018), the functional neuroimaging literature on patients with gliomas is highly diverse as regards techniques. So far, there has been no systematic assessment of how methodological choices impact observed results.

Methodological choices arise at multiple stages of fMRI data analysis. First, a primary focus of FC investigations in glioma patients concerns potential reorganization of RSNs (Lv et al., 2022). Accurate assessment of RSN topography depends on accurate registration of the functional data to an atlas template, e.g., MNI152 (Fonov et al., 2009). This is achieved via a sequence of steps, beginning with atlas registration of the patient's structural data. Although recent results show that non-linear registration of structural data to the atlas is preferred in patients with gliomas (Chen et al., 2021), the downstream effects of alternative atlas registration strategies on measures of FC remain incompletely addressed. Second, once the functional data are accurately registered to the atlas template, FC is computed by correlation analysis of time series extracted from regions of interest distributed throughout the brain. For this analysis to be maximally informative, the parcels from which the time series are extracted should match the functional organization of the brain. The influence of alternative parcellation schemes on the inferences derivable from rs-fMRI has not so far been examined. Third, it is well established that RSNs are hierarchically organized (Doucet et al., 2011; Gotts et al., 2020). The distinction between unimodal vs. trans-modal (alternatively, task-positive vs. task-negative) functional systems defines the top of the hierarchy (Doucet et al., 2011; Fox et al., 2005; Huntenburg et al., 2018; Lee et al., 2012). This dichotomy can be further subdivided into progressively finer parcels according to a variety of schemes (Gordon et al., 2016; Schaefer et al., 2018; Yeo et al., 2011). Consequently, the degree to which RSN organization is abnormal in glioma patients theoretically depends on the granularity of the parcellation. This issue has never before been investigated. Lastly, the glioma-dependent changes in RSN structure have been investigated using a variety of graph-theoretic measures (Bullmore and Sporns, 2009; Rubinov and Sporns, 2010). Which of these measures best captures the characteristic abnormality in glioma patients, as well as the downstream effects of the above-mentioned methodological choices remains uncertain.

Thus, our current work primarily focuses on technical optimization of rs-fMRI analysis in glioma patients and is fundamentally different from the bulk of papers relating glioma-induced functional network changes to clinical outcomes. We begin this work by conducting a systematic review of the literature (presented in Supplemental Materials, Table S1). Importantly, we focus on the following aspects of FC analysis in glioma patients: (1) atlas registration; (2) parcellation scheme; (3) parcel granularity; and (4) graph-theoretic measures. Specifically, we perform group-level analyses of data representing 163 healthy adults from the Open Access Series of Imaging Studies (OASIS3) dataset (LaMontagne et al., 2019) and 59 glioma patients from Washington University School of Medicine (WUSM) neurosurgery brain tumor database. First, we compare affine vs. non-linear atlas registration with and without tumor masking and evaluate the impact of these alternatives on the quality of structural normalization. Next, we assess the influence of different parcellation schemes (AAL vs. Brainnetome vs. Schaefer) on several measures of FC. We then evaluate how parcel granularity impacts the differentiation of patients from reference subjects on the basis of whole-brain FC measures and graph-theoretic measures. Finally, we analyze the impact of different atlas registration options on parcel-based measures of FC abnormalities in glioma patients. In the Discussion, we relate our review of the current literature to the present findings.

## 2. Methods

An overview of the entire analytic scheme used in this work is represented in Fig. 1 and Fig. S5.

### 2.1. fMRI Datasets

#### 2.1.1. Glioma dataset

The patient dataset comprised 59 glioma patients aged 22 – 82 years (average 58 years), retrospectively identified in the Washington University School of Medicine (WUSM) neurosurgery brain tumor database (dates acquired: 10/2012 – 5/2017). Inclusion criteria included: a new diagnosis of primary glioblastoma; age above 18 years; MRI at WUSM including fMRI for presurgical planning; and adequate tumor segmentation (i.e., no false labeling of normal tissue as tumors) (Section 2.2.1). Exclusion criteria included: prior brain surgery or inability to have an MRI scan. All analyses were conducted retrospectively using preoperative data. Owing to the retrospective nature of the study, informed consent was waived by the Washington University Institutional Review Board. Patients were scanned with either a 3 T Trio or Skyra scanner (Siemens, Erlangen, Germany) using a standard clinical presurgical

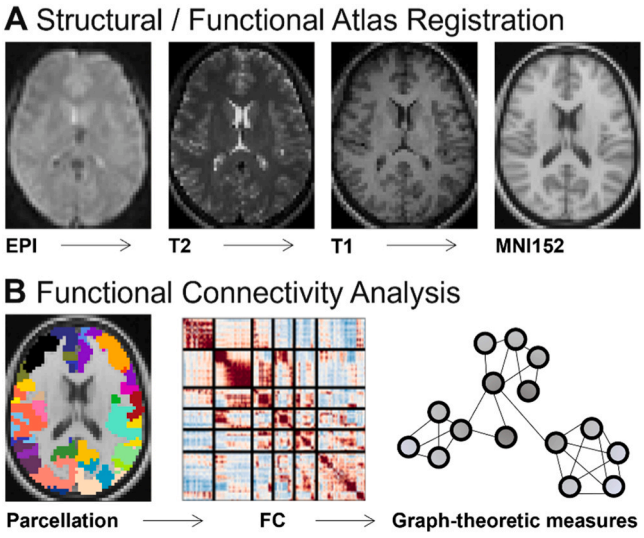


**Fig. 1.** Analysis pipeline. **A. Structural/Functional Atlas Registration.** The BOLD fMRI data are resampled in atlas space using the transform obtained via the sequence: EPI → T2 → T1 → MNI152. **B. Functional Connectivity Analysis.** A functional connectivity matrix is computed using fMRI time series extracted from the parcels. The illustrated matrix was obtained using the Schaefer parcellation (left most panel). Graph-theoretic measures of FC are applied to the obtained FC matrix results. Detailed information regarding structural and functional registration is included in Supplemental Materials.

tumor protocol. Anatomical imaging included a T1w magnetization prepared rapid acquisition (MP-RAGE), a T2w fast spin echo, and a FLAIR (Fluid-attenuated inversion recovery) image, all with a voxel size of $(1\ mm)^3$ were used for tumor segmentation. rs-fMRI was acquired using a BOLD-sensitized EPI (Echo-planar imaging) sequence (voxel size $(3\ mm)^3$ isotropic; echo time = 27 ms; repetition time = 2.2 – 2.9 s; field of view = 256 mm; flip angle = 90°). Two rs-fMRI runs were obtained in each patient (320 frames total); each run included 160 frames. All aspects of this study were overseen by the Washington University Institutional Review Board to ensure appropriate patient confidentiality.

#### 2.1.2. Reference dataset

The reference group comprised 163 individuals (43 – 93 years, average 67 years) selected from among 1098 participants in the OASIS-3 dataset (LaMontagne et al., 2019) to achieve age-matching with the patient group. Inclusion criteria were: first scan of the participants who had Clinical Dementia Rating (CDR) score of zero at every assessment; MRI acquired with Siemens TIM Trio 3 T scanner; presence of at least two rs-fMRI runs plus T1-weighted (T1w) and T2-weighted (T2w) structural images. The resting state fMRI data included two 6-minute runs (328 frames) acquired while participants were asked to remain still with their eyes open (voxel size $(3\ mm)^3$ isotropic; echo time = 27 ms; repetition time = 2.2 or 2.5 s).

### 2.2. Atlas registration

#### 2.2.1. Tumor segmentation for cost-function masking

Automated tumor segmentation was performed by a pre-trained 3D convolutional neural network (CNN) (Isensee et al., 2017) using post-contrast T1-weighted (T1w), T2w, and FLAIR images (details in Supplemental Materials S2.1.). The T2w and FLAIR images were rigid body registered to the T1w. All images were resampled in atlas space after composition of transforms: T2w → T1w → atlas template. Tumor segmentation was carried out in atlas space. The algorithm produces a multi-class tumor segmentation distinguishing between vasogenic edema, necrotic/non-enhancing core, and enhancing core. Tumor segmentations were visually inspected to verify accurate delineation of the tumor and transformed back into the patient space. Adequate tumor segmentation was an inclusion criterion (Section 2.1.1). In subsequent atlas registration of both anatomical and functional data, the cost-function mask included all three tumor classes.

#### 2.2.2. Atlas registration with cost-function masking

We systemically compared three alternative atlas registration strategies: (i) 12-parameter affine registration with no masking (*AFF*); (ii) Non-linear registration with no masking (*NL-M*); (Dobelbower et al.) Non-linear registration with cost function masking (*NL+M*). Preliminary investigations demonstrated that skull stripping did not improve atlas registration and so was omitted in this analysis. All atlas transformations were initialized by 12-parameter affine transformation of the patient's T1w to the MNI152 template (Fonov et al., 2009). The Advanced Normalization Tools (ANTs) diffeomorphic algorithm (https://www.nitrc.org/projects/ants) with symmetric normalization (Lindner et al.) was applied in conjunction with either no masking (*NL-M*) or whole tumor masking (*NL+M*). We used mutual information as the optimization metric. The transformation matrix and deformation fields obtained from the affine and non-linear registration steps were composed to obtain the transformation of structural images to atlas space (Fig. S5A, B).

### 2.3. fMRI preprocessing

Initial fMRI preprocessing followed conventional practice (Shulman et al., 2010). Briefly, this included compensation for slice-dependent time shifts, elimination of systematic odd-even slice intensity differences due to interleaved acquisition and rigid body correction of head movement within and across runs (Power et al., 2012). The fMRI data were resampled in atlas space using composition of affine transforms, i.e., functional data average → T2w → T1w → atlas template (Fig. 1). The warping maps (Section 2.2.2.) then were applied to the previously obtained affine transformed fMRI data and resampled in $(3\ mm)^3$ atlas space (Fig. S5B).

Additional preprocessing in preparation for FC analysis included voxel-wise removal of linear trends over each fMRI run, temporal low-pass filtering retaining frequencies below 0.1 Hz, and regression of nuisance waveforms. Nuisance regressors were derived from the 6 head motion correction timeseries, timeseries extracted from regions in white matter and CSF (Behzadi et al., 2007), and the signal evaluated over the whole-brain. Finally, spatial smoothing was applied (6 mm full width at half maximum (FWHM) Gaussian blur in each direction) (Fig. S5B).

Frame censoring was implemented using the DVARS (D refers to temporal derivative of timeseries; VARS refer to RMS variance over voxels) measure, which quantitates the root mean squared variance of the temporally differentiated fMRI data evaluated over the whole brain (Power et al., 2012; Smyser et al., 2010). The DVARS baseline exhibits subject-to-subject variability that currently is unexplained but may reflect fluctuating arterial $pCO_2$ (Power et al., 2019). The present frame censoring strategy accommodates DVARS baseline variability. A detailed description of the algorithm is given in Supplemental Materials (S2.2.).

### 2.4. Resting state networks and parcellations

#### 2.4.1. Schaefer parcellation

Resting state networks (RSNs) are hierarchically organized at multiple levels of granularity (Doucet et al., 2011; Felleman and Van Essen, 1991; Gotts et al., 2020; Kaas, 1987; Lee et al., 2012; Yeo et al., 2011). This organization theoretically affects the degree to which gliomas induce FC abnormalities. Accordingly, we systematically varied the coarseness of parcellations. The coarsest level corresponded to the 7 RSN solution reported by Yeo et al. (2011). Finer RSN parcellations were as reported by Schaefer and colleagues (Schaefer et al., 2018), comprising a variable number of parcels ranging from 100 to 1000 (Schaefer et al., 2018).

#### 2.4.2. Alternative parcellation schemes

We conducted a comparative analysis of alternative parcellation schemes commonly used in glioma neuroimaging research. The AAL parcellation (83 parcels) is based on anatomical features, primarily sulci, as imaged on T1w scans (Tzourio-Mazoyer et al., 2002). The Brainnetome parcellation (210 parcels) is based on the combination of automatic parcellation, tractography, and functional connectivity analysis (Fan et al., 2016). Only cortical regions in Brainnetome parcellation were used in the present analysis. We conducted several analyses to evaluate the impact of parcellation granularity on measures of FC. In those analyses, AAL and Brainnetome granularities comparable to the Schaefer scheme were based on parcel count.

### 2.5. Functional connectivity

At each level of RSN granularity, resting state FC was computed from the preprocessed data in atlas space (affine or non-linearly registered) resampled to $(3\ mm)^3$ voxels. In greater detail, FC was computed as the Fisher z-transformed Pearson temporal correlation between timeseries extracted from individual parcels. Thus, FC was evaluated in terms of $L \times L$ symmetric matrices, where $L$ is number of parcels corresponding to a particular level of granularity (see Section 2.4. for details).

### 2.6. Evaluation of Atlas Registration – structural similarity

Each patient's atlas transformed T1w image was compared to the MNI152 template. Quality of structural normalization was assessed

using the structural similarity (SSIM) index (*ssim* function in Matlab) between the transformed individual T1w images and the MNI152 template, excluding voxels in the tumor mask. The SSIM index is a multiplicative combination of three separate comparisons: average pixel intensities, standard deviations in the images, and the cross-covariance structure in the images (Wang et al., 2004).

### 2.7. Graph-theoretic measures

We evaluated the impact of parcellation scheme and parcellation granularity on graph-theoretic measures. Prior analyses had established that affine atlas registration failed to achieve adequate matching of structural data to the atlas (Fig. 2B). Accordingly, we evaluated parcellation schemes using functional data preprocessed with non-linear registration and cost-function masking (NL+M). For each parcellation scheme and parcellation granularity, we evaluated graph-theoretic measures on binarized graphs derived from FC matrices as a function of graph density (10–30% at 2% intervals). In accordance with current conventional practice (Bullmore and Sporns, 2009; Rubinov and Sporns, 2010), graph edges were defined only for positive correlations. We assessed three graph-theoretic measures commonly evaluated in the rs-fMRI literature using the Brain Connectivity Toolbox [http://www.brain-connectivity-toolbox.net]:

1. *Modularity*. Modularity is a whole-graph measure that quantifies the degree to which the network can be segregated into discrete groups (Newman, 2004).

2. *Global Efficiency*. Global Efficiency is a whole-graph measure that evaluates the average inverse shortest path length (Rubinov and Sporns, 2010).

3. *Mean Clustering Coefficient*. Clustering coefficient measure is based on the number of triangles present in the network (Rubinov and Sporns, 2010). A large number of triangles suggest segregation, as the fraction of triangles around a node is known as the Clustering Coefficient (CC) and is equivalent to the fraction of the node's neighbors that are also mutual neighbors. The mean CC for the global network reflects, on average, the prevalence of clustered connectivity around individual nodes.

### 2.8. Statistical analysis

#### 2.8.1. Full-width Half Maximum (FWHM) analysis as a measure of FC robustness

The distribution of FC values following global signal regression is approximately zero-centered (Fox et al., 2009). Thus, robust FC is characterized by the presence of both strong positive and strong negative correlations evaluated over all parcel pairs. Accordingly, the width of FC distributions compiled over all parcel pairs is a measure of FC robustness. We evaluated the width of FC distributions as the Full Width at Half Maximum (FWHM).

#### 2.8.2. Permutation testing of graph-theoretic differences across groups

We assessed the impact of parcellation scheme and parcellation granularity on group differences (glioma patients vs. reference subjects) evaluated in terms of graph-theoretic measures (see Section 2.7). We evaluated differences in group means and assessed statistical significance using permutation resampling (N = 2000) as previously described (Alexander-Bloch et al., 2012). Thus, the p-value is computed as the number of instances in which the actual group difference exceeds that in the null distribution obtained by permuting group assignments over subjects, divided by the number of permutations. Multiple comparisons correction was conducted as previously described (Alexander-Bloch et al., 2012) depending on the context of the comparison. Specifically, the combination of parcellation granularity options and graph density options were used as multiple comparisons to correct for false positives (i.e., N granularity options × M graph density options yield N × M multiple comparisons, $p < 1/(N \times M)$).

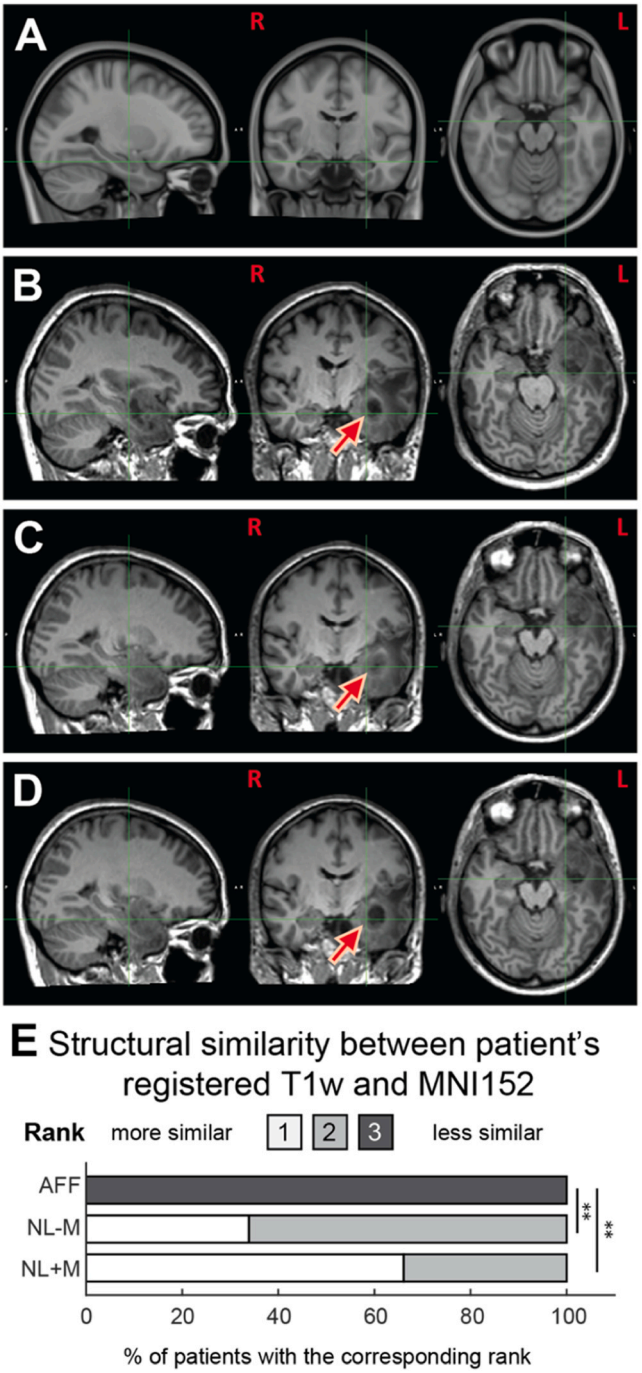


**Fig. 2.** T1w structural normalization. **A.** MNI152 template. **B.** Result obtained using affine only (AFF) registration. **C.** NL-M: Non-linear registration without masking. Note tumor shrinkage. **D.** NL+M: Non-linear registration with masking. Note absence of tumor shrinkage. **E.** Friedman rank-sum and Nemenyi posthoc test results for structural registration quality (see Supplemental section S3.1). Structural similarity to the MNI152 is evaluated using methods described in Section 2.6. For each patient, the similarities using three methods (AFF vs. NL-M vs. NL+M) are ranked from 1 to 3, with a lower rank corresponding to better quality. In all patients, the lowest similarity was observed with AFF, as demonstrated by 100% of patients showing rank = 3 for AFF. NL-M achieved the best results in 36% of patients. NL+M achieved the best results in 64% of patients. * * Nemenyi score > 0.43 (see Section 2.8.5 and Supplemental S3.1).

#### 2.8.3. Similarity index

Resting state networks (RSNs) are hierarchically organized at multiple levels of granularity (Doucet et al., 2011; Felleman and Van Essen, 1991; Gotts et al., 2020; Kaas, 1987; Lee et al., 2012; Yeo et al., 2011). Thus, apparent FC variability across healthy individuals depends on parcel granularity. Specifically, FC differences across normal as well as abnormal individuals are expected to be most apparent at fine parcel granularities. We define the Similarity Index as a measure of inter-subject FC variability and evaluate this measure parametric in parcellation granularity (Fig. 4). FC similarity was evaluated in terms of inner products of vectorized FC matrices. Additional algebraic details concerning the Similarity Index and the analytic rationale are provided in Supplemental Materials (S3.2. and S3.2.1.).

#### 2.8.4. Patient vs. reference group dissimilarity index

The Dissimilarity Index is a quantitative measure at the group level that represents the degree to which whole-brain FC differences between glioma patients and the reference subjects exceeds normal variability in the reference dataset. We anticipate that the Dissimilarity Index strongly depends on parcellation granularity. To evaluate the Dissimilarity Index, we first compute FC matrices for all subjects and patients. We then evaluate FC similarity across all subject pairs in the reference group vs. all ways of pairing a patient with all subjects in the reference group. This computation gives rise to two histograms, illustrated in Fig. 4A. Additional analytic details are given in Supplemental section S3.3. We quantify the Dissimilarity Index as the D-statistic from the two-sample Kolmogorov-Smirnov test (used descriptively), which reflects the degree to which two distributions differ (Fig. 4C). The Dissimilarity Index was evaluated across all levels of the Schaefer parcellation granularity (7, 100–1000 with 100 intervals). Additional algebraic details concerning the Dissimilarity Index and the logical reasoning are provided in Supplemental Materials (S3.2., S3.2.2., Fig. S4).

#### 2.8.5. Rank-based non-parametric test: Statistical Comparison of Atlas Registration and Parcellation Scheme

Three registration options – *AFF, NL-M,* and *NL+M* – were systematically compared. Quality of spatial normalization (Section 2.6.1) was evaluated separately from quality of functional registration (Section 2.8.6). As the patient dataset was markedly heterogeneous with respect to tumor size and location, the three registration options were compared using the Friedman non-parametric test (Eisinga et al., 2017), which measures the consistency of registration option rank across patients and returns a test statistic, Q, distributed approximately as chi-squared. The Friedman test was used to evaluate the dependence on registration option of both structural and functional data. The Nemenyi posthoc test (Nemenyi, 1963) was used to assess the significance of differences between the 3 options taken pairwise.

We also systematically compared 6 parcellation schemes (AAL, Brainnetome, and 4 Schaefer parcellations at differing granularity levels) using FWHM analysis (see Section 2.8.1). Given the marked heterogeneity of tumors, the same Friedman non-parametric test was used, with the Nemenyi posthoc test to ascertain significance between pairwise differences. Further details concerning the Friedman non-parametric and Nemenyi posthoc tests are provided in Supplemental Materials (S3.1).

#### 2.8.6. Evaluation of atlas registration options based on measures of functional connectivity

*2.8.6.1. Parcel homogeneity.* If parcel boundaries are well-aligned with the functional organization of the brain, all voxels in a given parcel should exhibit similar functional connectivity. A measure of this similarity is referred to as parcel homogeneity (Gordon et al., 2016). We evaluated parcel homogeneity as previously described (Gordon et al., 2016). In brief, this entails computing the whole-brain connectivity pattern for each voxel in a parcel. Parcel homogeneity is defined as fraction of variance in the first eigenvector derived by principal component analysis (PCA) of whole-brain FC computed for all voxels in the parcel. Thus, if the parcel contains n voxels, PCA is applied to the n FC maps corresponding to each voxel. Parcel homogeneity was computed for all atlas registration options (AFF, NL-M and NL+M).

*2.8.6.2. Parcel aberrancy.* We define Parcel Aberrancy for each parcel as the FC differences in the patient group relative to the reference group in excess of (normal) variability in the reference group. The computation of Parcel Aberrancy follows a similar approach to computing the Dissimilarity Index, as outlined in Section 2.8.4. The key difference is that we evaluate parcel-specific FC as opposed to the FC over the entire matrix (details included in Supplemental Materials, S3.3). Moreover, we quantify the Parcel Aberrancy score using Kolmogorov-Smirnov D statistic, which provides a measure of the extent to which the two distributions differ. Parcel Aberrancy was evaluated for all atlas registration options, but only for the Schaefer parcellation at the finest granularity (1000 parcels).

Ideally, Parcel Aberrancy should reflect true FC differences attributable to the glioma. However, Parcel Aberrancy can arise on the basis of suboptimal atlas registration. To disambiguate the origin of observed Parcel Aberrancy, we compare Parcel Aberrancy vs. parcel homogeneity under alternative atlas registration options (Fig. 5C). A detailed description of these computations is given in Supplemental Materials (S3.3 and Fig. S4).

## 3. Results

### 3.1. Spatial normalization with different atlas registration options

The impact of alternative atlas registration strategies is illustrated in Fig. 2. Visual inspection of spatial normalization results obtained with the different methods revealed differences in proximity to the lesion (see Fig. 2; arrows). Specifically, *AFF (affine registration)* (Fig. 2B) preserves tumor proportions relative to the rest of the brain. *NL-M* (non-linear registration without masking) (Fig. 2C) shrinks the lesion, distorts nearby regions, and blurs the tumor boundary. Using *NL+M* (non-linear registration with masking) (Fig. 2D) preserves the relative proportions of the tumor, as in the *AFF* result, while warping the rest of the brain to match the template more closely than affine registration. Panel E reports a significant effect of atlas registration option on structural normalization (Friedman rank test, $p = 1.31e\text{-}20$). Tumor voxels were excluded in this evaluation. Additionally, the Nemenyi posthoc test results highlighted that using non-linear registration significantly improves structural similarity compared to using affine registration (asterisks in Fig. 2E). The impact of masking was not significant.

### 3.2. Impact of parcellation scheme on FC matrices and graph-theoretic network measures

Fig. 3 represents the effects of parcellation scheme and parcellation granularity on the width of FC distributions and graph-theoretic measures. Fig. 3A illustrates the AAL, Brainnetome, and Schaefer parcellation schemes overlaid on the atlas template. We compared the robustness of FC evaluated using 6 different parcellation schemes (AAL vs. Brainnetome vs. Schaefer schemes at varying granularities). FWHM was used as a measure of FC robustness (Fig. 3B). The FWHM analysis shows that parcellation schemes that are well matched to the functional organization of the brain give rise to robust FC (i.e., large FWHM). Conversely, parcellation schemes that are poorly matched to the functional organization of the brain generate weaker FC (i.e., low FWHM). The rank order of each of the schemes is represented as box plots (lower rank indicates greater FWHM value). All of the results are plotted as a function of parcel count. At equivalent levels of parcellation granularity,

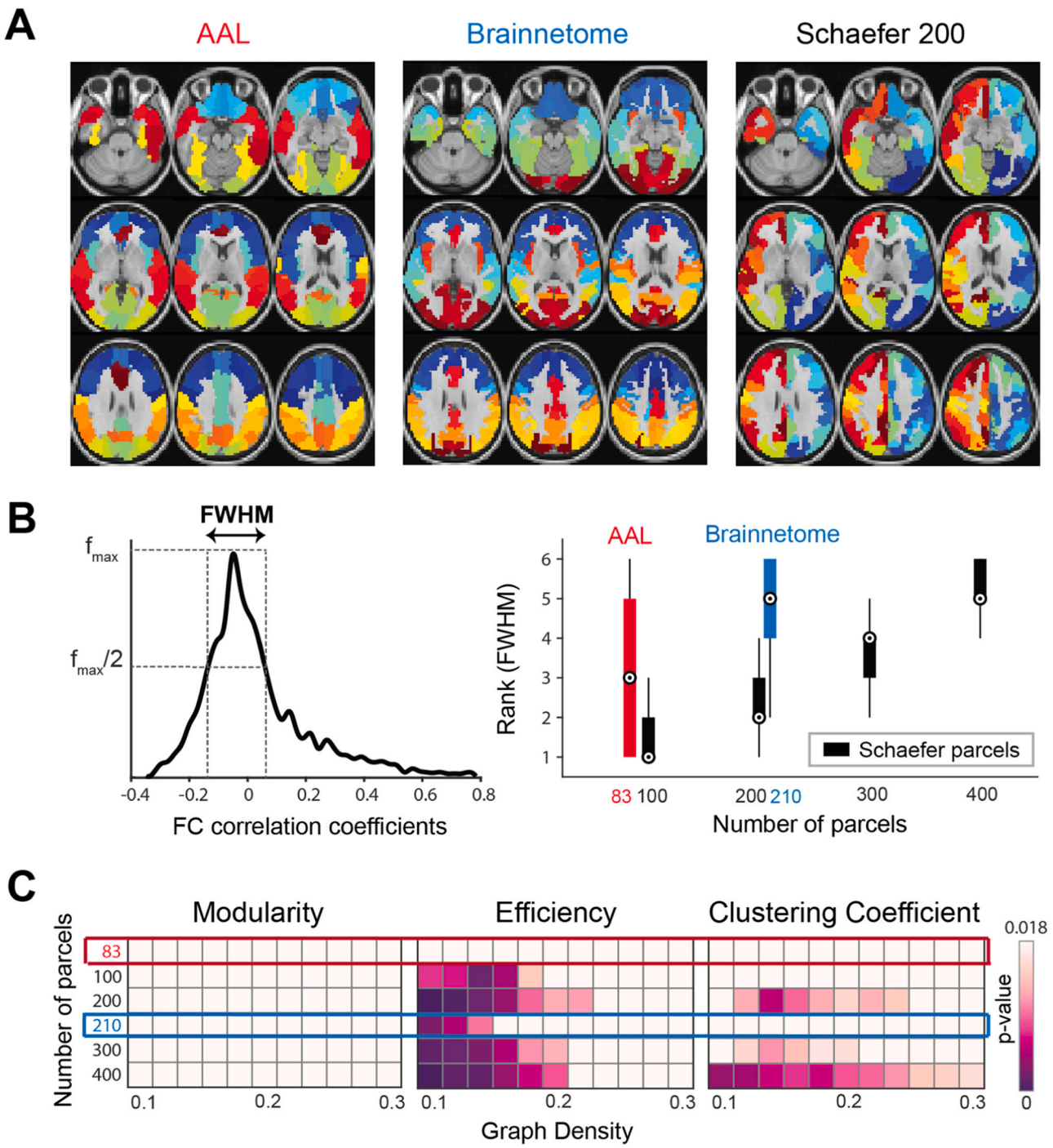


**Fig. 3.** Impact of parcellation scheme on functional connectivity matrices and graph theoretic network measures. **A.** Parcellation examples illustrating AAL, Brainnetome, and Schaefer 200. **B left.** Full Width at Half Maximum (FWHM) of correlation matrix value distributions obtained with different parcellation schemes. **B right.** Rank order of FWHM values across six parcellations. The boxplots represent rank distributions compiled over 163 reference subjects. Low rank signifies comparatively greater FWHM. The height of each boxplot represents the standard deviation of ranks across subjects. Rank mean is represented as a circle. Note systematically decreasing FWHM (higher rank) with increasing granularity of Schaefer parcels (black boxplots). Both AAL and Brainnetome show higher rank (narrower FWHM) than comparably sized Schaefer parcellations. **C.** Impact of parcellation scheme on significance of group differences evaluated using graph theoretical measures. The display illustrates the effects of both graph density and parcellation granularity. Red and blue rows show results obtained using the AAL3 and Brainnetome parcellations, respectively. Black rows correspond to graded Shaefer parcellations. Note complete absence of significant group differences in Modularity as assessed with any parcellation. Note absence of significant group differences in any measure assessed with the AAL parcellation (red row). Note significant Brainnetome differences only for Efficiency and only at sparse graph densities. Significant group differences in Efficiency and Clustering Coefficient were obtained with Schaefer parcellations at low graph densities and finer granularities.

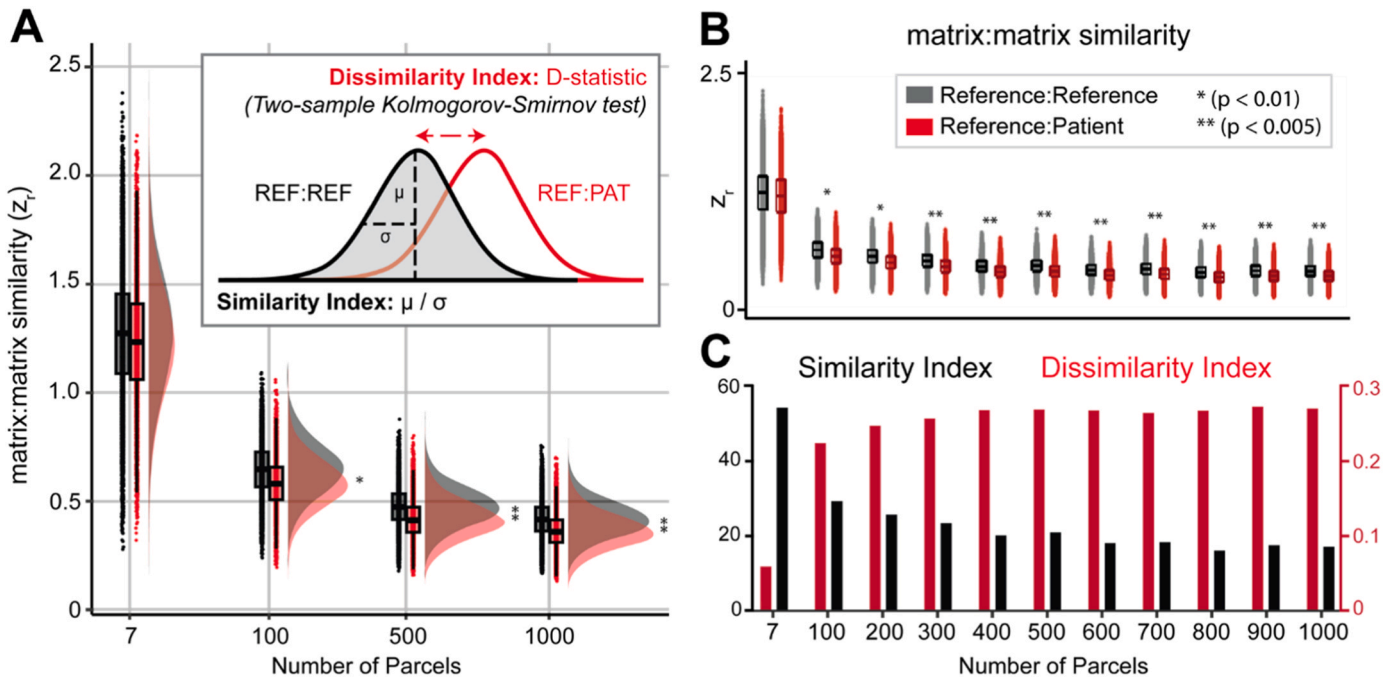


**Fig. 4.** Impact of Parcellation Granularity on Functional Connectivity Consistency and Group Separation. **A, B.** Pairwise FC matrix similarities within the 163 reference subjects (grey) and between these reference subjects and the 59 patients (red). * $p < 0.01$, * * $p < 0.005$ (see Supplemental Materials 3, Fig. S4 for details). In the inset illustrating histogram overlap, the ":" notation indicates matrix:matrix similarity computed as Pearson correlation over vectorized FC matrices. **C.** Similarity Index is measured as the average of pairwise FC similarity values within reference subjects divided by the standard deviation of these values (grey distribution shown in the top panel). Dissimilarity Index is evaluated as the D-statistic from a two-sample Kolmogorov-Smirnov test, contrasting pairwise similarity values within reference subjects (grey distribution in the top panel) and those between reference subjects and patients (red distribution in the top panel). Additional algebraic details concerning both indices and the logical reasoning are provided in Supplemental Materials (S3.2. and Fig. S4).

the Schaefer scheme consistently yielded more robust FC in comparison to AAL and Brainnetome (Fig. 3B). This result suggests that the Schaefer parcellation scheme most closely conforms to the functional organization of the human brain. As a generality, the robustness of FC is greater at coarser parcellations, although this relation is most systematic with the Schaefer scheme.

Fig. 3 C shows the impact of parcellation scheme and parcellation granularity on the difference between patients and reference subjects evaluated using three graph-theoretic measures: Modularity, Global Efficiency, and Mean Clustering Coefficient. The significance of the contrast between the two groups was evaluated parametric in graph density and parcel granularity. Inspection of Fig. 3C shows that the contrast between patients and reference subjects was greatest at sparse graph densities and finer parcellation granularities. Of the three graph-theoretic measures examined, group differences were most apparent in the Global Efficiency measure. Finer Schaefer parcellations and the Brainnetome scheme both yielded significant group differences in Global Efficiency at sparse graph densities. The Mean Clustering Coefficient also yielded significant group differences, but only with the Schaefer scheme. The Brainnetome scheme was inferior to the Schaefer scheme at the comparable granularity (Fig. 3C, blue box, middle panel). Specifically, significant Brainnetome differences were apparent only in efficiency and only at sparse graph densities. Notably, the AAL parcellation yielded no significant group differences using any graph-theoretic measure at any graph density (Fig. 3C, red box). Fig. S7 extends these results, focusing on the Schaefer parcellation scheme in greater detail.

### 3.3. *Whole-brain group contrast in FC parametric in parcellation granularity*

Fig. 4A represents histograms of FC similarity evaluated within and across groups. The grey histograms represent all pairs of reference subjects. The red histograms represent all ways of pairing patients with reference subjects. At parcellation granularities greater than 100, FC matrix similarity was greater within group (reference subjects only) as compared to across groups (two-sample Kolmogorov-Smirnov test, asterisks graded based on D-statistic; Fig. 4B). This is represented in Fig. 4A as a shift of the grey histogram relative to the red histogram. Note that the FC difference between the patient and the reference group was not significant at the coarsest parcellation (7 parcels) but became progressively more pronounced with increasing parcel count.

Fig. 4C shows both within reference group similarity (black bars) and across group dissimilarity (red bars) parametric in parcellation granularity. Within reference group similarity was greatest at the coarsest parcellation and systematically declined with increasing granularity (black bars). Across group dissimilarity showed the inverse dependence on parcel count (red bars) but leveled off at a parcel count of ~400. Thus, this result suggests that differentiating glioma patients from reference subjects on the basis of whole brain FC improves with increasing granularity up to a certain level.

### 3.4. *Parcel homogeneity and aberrancy computed with different atlas registration options*

The current results indicate that FC dissimilarity becomes increasingly apparent with finer parcellation granularities (Fig. 4). In view of this finding, we extended our analysis to contrast the two groups at the finest parcellation level, identifying functionally altered brain regions in patients. Accurate quantitation of FC abnormalities at the parcel level depends on precise alignment of parcel boundaries with the true functional organization of the brain, which is evaluated in Fig. 5A as Parcel homogeneity (see Section 2.8.6.1. for details).

Fig. 5A illustrates the impact of alternative atlas registration strategies on parcel homogeneity in the patient group. Parcel homogeneity is parcel-dependent and tends to be greatest in primary sensory/motor areas of the brain, and least in multimodal regions such as prefrontal

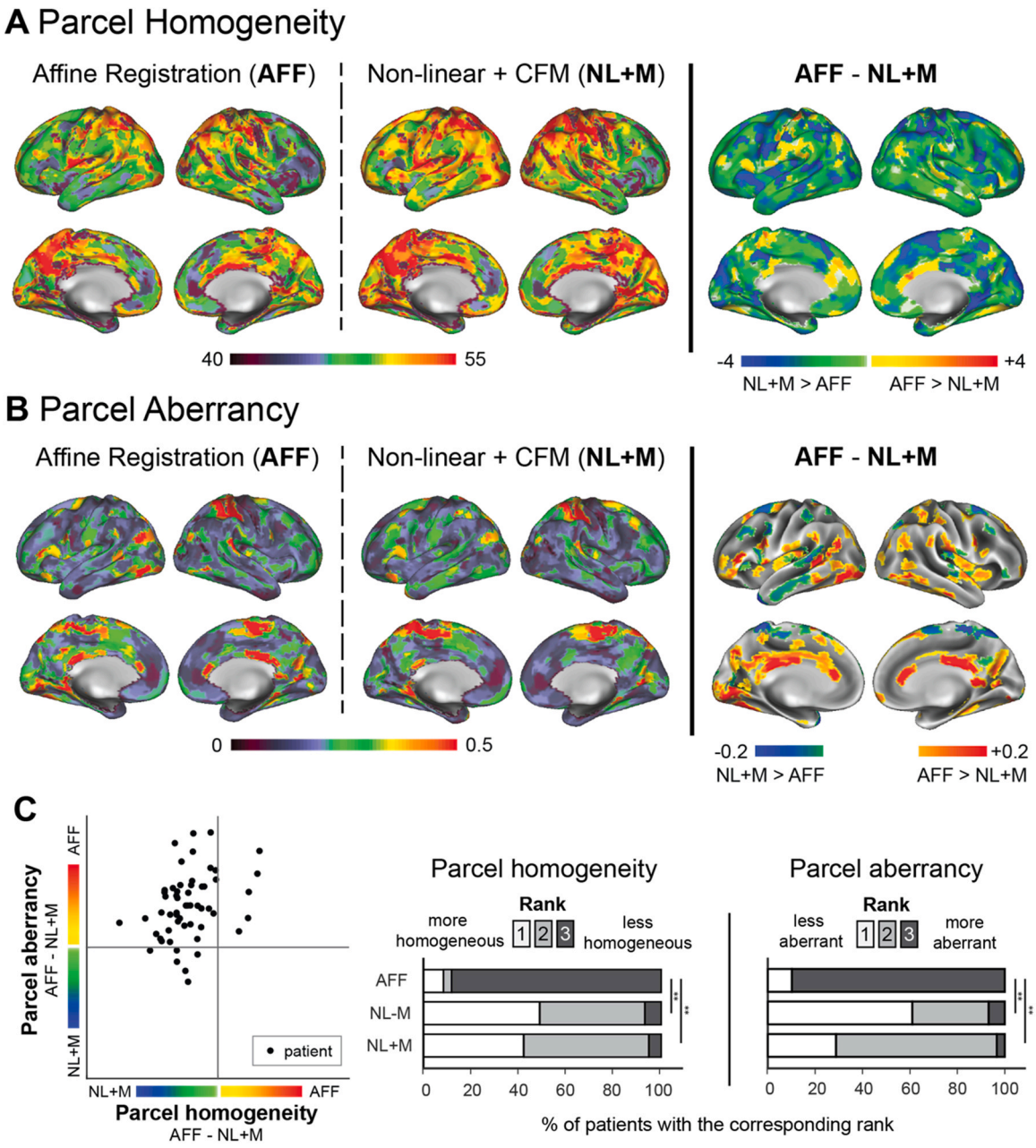


**Fig. 5.** Impact of atlas registration option on parcel homogeneity and parcel aberrancy. **A.** Parcel homogeneity. Results using affine registration (AFF) and non-linear registration with masking (NL+M) are displayed (left of the solid bar), along with their differences (right of the solid bar). Blue/green regions show greater homogeneity with NL+M; red/yellow regions indicate greater homogeneity with AFF. **B.** Parcel aberrancy. Results using affine registration (AFF) and non-linear registration with masking (NL+M) are displayed (left of the solid bar), along with their differences (right of the solid bar). Blue/green regions show greater aberrancy evaluated with NL+M; red/yellow regions indicate more aberrancy evaluated with AFF. **C.** Friedman rank-sum and Nemenyi posthoc test results. Lower ranks represent higher parcel homogeneity and less parcel aberrancy. Most patients showed the least homogeneity and most aberrancy with AFF. Highest homogeneity and least aberrancy were found comparably with non-linear registration with and without masking (NL-M, NL+M). * * Nemenyi score $> 0.43$ (see Supplemental Materials S3.1.).

cortex (left two panels in Fig. 5A). The rightmost panel displays the difference in parcel homogeneity. Non-linear atlas registration generally improves parcel homogeneity in all parcels (cooler hues). This qualitative assessment was quantitatively verified using the Friedman rank test ($p = 6.14e\text{-}13$) and Nemenyi posthoc test (asterisks in Fig. 5C).

Parcel Aberrancy is equivalent to the Dissimilarity Index (see Section 2.8.6.2) restricted to one row of FC matrices (see Supplemental section S3.3). The above discussed results concerning the impact of atlas registration on parcel homogeneity imply that the ability to detect true parcel FC aberrancy depends on accurate atlas registration. Inaccurate atlas registration can lead to the false appearance of FC abnormalities. This result is illustrated in Fig. 5B. Specifically, affine atlas registration led to inflated Parcel Aberrancy scores, especially in the cingulate cortex (red hues on the rightmost panel). This effect most likely reflects the inability of affine registration to correct for midline shift, which is common in glioma patients. The inverse (AFF $<$ NL+M) result was observed in the left temporal lobe (green parcels on the rightmost panel). Tumor frequency was left-lateralized in our patient sample (Fig. S7). Thus, hypothetically, increased sensitivity for the detection of FC aberrancy in the left temporal lobe with NL+M atlas registration

reflects true aberrancy in parts of the brain immediately adjacent to the tumor. This hypothesis could be verified in future work.

The link between parcel homogeneity and Parcel Aberrancy is illustrated in the leftmost panel of Fig. 5C, which shows a scatter plot across patients. Non-linear atlas registration generally improved parcel homogeneity (most patients positioned left of the vertical line) and reduced Parcel Aberrancy (most patients positioned above the horizontal line). This result reinforces the result shown in Fig. 5B, as improved atlas registration increases parcel homogeneity and decreases Parcel Aberrancy.

## 4. Discussion

### 4.1. Results overview

We evaluated the impact of atlas registration option, parcellation granularity, and parcellation scheme in the context of contrasting FC in glioma patients vs. a group of age-matched reference subjects. Differences between the two groups strongly depended on these methodological choices. Our key findings are as follows: (1) Non-linear atlas registration is required to compensate for anatomical distortions in glioma-bearing brains. Use of affine atlas registration leads to the false appearance of FC abnormalities. Theoretically, cost function masking could impact the results. However, in our results, the impact of cost function masking was not significant. (2) Functional parcellation schemes, e.g., (Schaefer et al., 2018), as opposed to anatomical parcellation schemes (AAL/Brainnetome) maximize sensitivity for the detection of glioma-induced FC abnormalities (Fig. 3). (3) FC variability in normal subjects must be considered when assessing FC abnormalities in glioma patients. This point is implicit in our Parcel Aberrancy mapping strategy. FC abnormalities in glioma patients are most evident in analyses based on fine parcellations (Fig. 4). (4) Much prior work evaluates FC in glioma patients using graph-theoretic measures (see Literature Review in Supplemental Material S1, Table S1). As previously noted, not all such measures are equally sensitive to FC abnormalities in glioma patients. In particular, Modularity appears to be unchanged in glioma patients. Importantly, the differences between patients and the reference subjects as assessed with graph-theoretic measures were only evident at fine parcellation granularities.

### 4.2. Present results in relation to the extant literature

Many studies have suggested optimal fMRI analyses for studying subjects without brain tumors. However, to our knowledge, no extant study has comprehensively addressed this issue in the context of rs-fMRI analysis in glioma patients. Moreover, there has been no systematic comparison of how alternative methods impact observed results. To address this gap, the present work focuses on technical optimization of rs-fMRI analysis in glioma patients. We began this work by conducting a systematic review of the literature (presented in Supplemental Material 1, Table S1). We found that prior work used a variety of atlas registration strategies, seed-based FC or Independent Component Analysis, a variety of parcellation schemes at differing levels of parcellation granularity, and a wide variety of graph-theoretic measures. The majority of studies that implemented seed-based FC approaches used anatomically derived parcellation schemes, e.g., AAL. Parcellation granularity varied from 7 network parcellations to voxel-level analyses. Additional details concerning the extant literature are discussed in Supplemental Materials. In what follows, we discuss the extant literature in light of the present findings. Importantly, we report that alternative technical approaches have major effects on observed results.

#### 4.2.1. Non-linear Atlas registration improves structural normalization and parcel homogeneity

Structural normalization (i.e., matching individual brains to an atlas representative template) in glioma patients is a non-trivial challenge owing to destruction of normal tissue and anatomical distortions consequent to mass effects. Non-linear registration with cost-function masking (CFM) and Glioma Image SegmenTation and Registration (GLISTR) (Gooya et al., 2012) have been suggested as a means of improving spatial normalization in patients with brain tumors. However, as noted in several review papers and in our own review (see Supplementary Materials 1, Table S1), the extant literature on FC in glioma patients is characterized by substantial heterogeneity in atlas registration methodology (Fox and King, 2018; Ghinda et al., 2018) (Table S1). Prior work (not in Table S1) has compared atlas registration methods but only as regards structural normalization (Brett et al., 2001; Crinion et al., 2007; Ripolles et al., 2012). In our review of the literature, we found only one report that systematically discusses the impact of atlas registration on FC measures (Chen et al., 2021). We concur with Chen and colleagues that non-linear atlas registration should be used when studying glioma patients and that cost function masking does not significantly impact the results. Importantly, Chen and colleagues used graph-theoretic measures derived from AAL-based FC (coarse anatomical parcellation) as the primary metric to evaluate the quality of atlas registration, which we have shown is suboptimal.

Functionally-based parcellation schemes, e.g., (Schaefer et al., 2018), conform to the intrinsic functional organization of the brain, whereas anatomically-based schemes, e.g., AAL (Tzourio-Mazoyer et al., 2002), do not (Craddock et al., 2012; Shen et al., 2013). As shown with our FWHM measure, non-functionally-based schemes lead to less robust FC estimates and reduce the sensitivity of FC analyses for detecting differences between patients vs. controls (Fig. 3). Accordingly, we assessed the quality of atlas registration in terms of parcel homogeneity (Gordon et al., 2016), which directly assesses parcellation match to the functional organization of the brain. In contrast, graph-theoretic measures do so only indirectly via degraded FC. Moreover, fine, as opposed to coarse parcellations, are more sensitive to misregistration and inter-subject variability (Fig. 4).

#### 4.2.2. Functionally-based parcellation schemes improve the robustness of FC

Prior work in healthy participants suggests that functionally-based as opposed to anatomically-based parcellation schemes (e.g., AAL) are better matched to the functional organization of the brain (Craddock et al., 2012; Gordon et al., 2016; Shen et al., 2013). This basic finding is replicated here (Fig. 3). Parcellation scheme strongly impacts the value of graph-theoretic measures, which potentially are of interest in the comparison of glioma patients vs. controls. However, to effectively realize this comparison, it is essential that the parcellation scheme be matched to the functional organization of the brain. In this context, anatomically-based parcellation schemes perform poorly, even after controlling for equivalent parcellation granularity (Fig. 3C). We note that 27 of 58 prior studies of FC in glioma patients used anatomically-based parcels (AAL/Brainnetome/Harvard-Oxford/Brodmann).

#### 4.2.3. FC abnormalities in glioma patients are apparent only at fine parcellation granularities

Resting State Networks (RSNs) are hierarchically organized (Doucet et al., 2011; Gotts et al., 2020). Accordingly, inferences drawn on the basis of FC analyses may depend on parcellation granularity. Various schemes incorporating progressively finer RSN subdivisions have been proposed (Schaefer et al., 2018; Yeo et al., 2011), but it is generally agreed that the distinction between unimodal vs. trans-modal (alternatively, task-positive vs. task-negative) systems defines the top of the hierarchy (Doucet et al., 2011; Fox et al., 2005; Huntenburg et al., 2018; Lee et al., 2012). In normal subjects, inter-individual differences in the functional organization of the brain are apparent predominantly at a fine spatial scale, i.e., on the order of several mm (Gordon et al., 2017). Our results suggest that a similar principle applies to FC abnormalities in glioma patients. Specifically, FC abnormalities are relatively inapparent at coarse parcellation granularities and become progressively more

apparent with increasing parcellation granularity (up to a point, Fig. 4C). However, we note that only 8 of 36 prior studies used a parcellation involving at least 200 parcels (Table S1).

#### 4.2.4. Graph-theoretic measures strongly depend on parcellation scheme and parcellation granularity

Approximately one-quarter of studies listed in Table S1 assessed the effects of glioma on the basis of graph-theoretic measures. Among these, all but one used anatomical parcellations (e.g., 7 used AAL atlas, 4 used Brainnetome atlas, and one defined ROIs based on anatomical landmarks); one defined ROIs based on mixed criteria. Our results, however, suggest that in the context of graph-theoretic analysis, anatomically-based parcellation schemes perform poorly compared to functionally-based parcellation schemes, even after controlling for equivalent parcellation granularity (Fig. 3C). Moreover, graph-theoretic measures strongly depend on atlas registration strategy (Chen et al., 2021). Additionally, we concur with the issues raised by Hallquist and colleagues regarding the use of graph-theoretic measures of FC in the evaluation of group differences (Hallquist and Hillary, 2019). Specifically, methodological heterogeneity across studies undermines the potential replicability of published findings (Hallquist and Hillary, 2019).

Here, we did not conduct an exhaustive comparison of all graph theoretic measures used in the literature (see Table S1). We did evaluate three commonly used measures, including Global Efficiency, a measure ubiquitous in glioma FC research (Section 2.7, Table S1). Importantly, we focus on evaluating graph-theoretic measures parametric in both parcellation granularity and graph density (Figs. 3C and S7). As far as we are aware, this experimental design is novel, as prior work has not systematically examined the impact of parcellation granularity. Our results support the use of Global Efficiency and Mean Clustering Coefficient as measures sensitive to the effects of glioma, provided the analysis is conducted using fine functional parcellations and at sparse graph densities (Fig. 3C and Fig. S7). The present observations open up new questions regarding how gliomas might induce functional reorganization. Answering those questions will require larger sample sizes to account for heterogeneity in grade of glioma and location of tumors.

#### 4.2.5. Non-linear Atlas registration reduces parcel aberrancy

Perhaps the most salient finding in the present work is that non-linear atlas registration generally reduces the appearance of FC abnormalities in glioma patients (Fig. 5). In contrast, affine atlas registration can lead to the false appearance of FC abnormalities attributable to misregistration. We note that 16 out of 58 studies contrasted glioma patients vs. controls using affine (or unspecified) atlas registration (Table S1). True FC abnormalities may arise from the destruction of normally functioning parenchyma or white matter, impaired neurovascular coupling (Ulmer et al., 2003), vasomotion (Rayshubskiy et al., 2014), and potentially, functional remapping (Lv et al., 2022). The present work does not distinguish between these possibilities.

#### 4.2.6. Limitations and caveats

Regarding non-linear atlas registration, it is possible that alternatives to ANTs, e.g., DARTEL, DRAMMS, or GLISTR may offer advantages (Ashburner, 2007; Gooya et al., 2012; Ou et al., 2011). Clinical imaging at our institution does not (at least at present) include field mapping or advanced methodologies designed to facilitate distortion correction. Thus, correction for susceptibility inhomogeneity was not possible in this work. Tumor frequency was left lateralized in our dataset, which is uncharacteristic of the glioblastoma population generally. Thus, our patient sample does not support a general examination of how tumors in different parts of the brain impact FC. For graph-theoretic analyses, we applied global thresholding to generate binarized FC matrices; future work could consider comparing global and local thresholding, as well as exploring other methods of graph construction. We compared one functionally-based parcellation scheme (Schaefer et al., 2018) to two anatomically-based schemes. Other functional parcellation schemes (Gordon et al., 2016; Power et al., 2011; Shen et al., 2013) may potentially enhance our understanding of tumor-induced FC changes. Lastly, unlike most prior work on FC abnormalities in glioma patients (Table S1), this work focuses on the technical aspects of this type of investigation with the objective of maximizing patient vs. control differences. We make no claims regarding specific FC abnormalities or functional reorganization in glioma patients. Such claims are deferred to future work with larger datasets.

## 5. Conclusion

Assessment of glioma-induced alterations in the functional connectome depends on methodological choices concerning structural normalization, parcellation scheme, and parcellation granularity. We reviewed commonly used approaches in rs-fMRI glioma literature and systematically assessed the impact of these choices on the observation of FC abnormalities in a group of glioma patients. Based on our findings, we offer several recommendations concerning the use of rs-fMRI to study patients with gliomas. First, non-linear atlas registration is required to compensate for anatomical distortions, which in turn, reduces the false appearance of FC abnormalities. Second, we recommend functional parcellation schemes over anatomical parcellation schemes to enhance sensitivity for the detection of true glioma-induced FC abnormalities. Third, measured FC variability in all subjects depends on parcellation granularity; this point should be considered when studying FC abnormalities in glioma patients. Importantly, FC abnormalities in glioma patients, as assessed with graph-theoretic measures, are most apparent at finer parcellation granularities.

## Funding

Cognitive, Computational, and Systems Neuroscience (CCSN) Fellowship, McDonnell Center for Systems Neuroscience, Washington University School of Medicine (KYP). National Institutes of Health grant R01CA203861 (KYP, JSS, PHL, ECL, AZS). National Institutes of Health grant P41EB018783 (ECL). National Institutes of Health grant U24NS109103 (ECL). National Institutes of Health grant R01EB026439 (ECL).

## CRediT authorship contribution statement

**Ki Yun Park, Abraham Z. Snyder**: Conceptualization, Formal analysis, Writing – original draft. **Ki Yun Park, Aaron B. Tanenbaum, Satrajit Chakrabarty**: Image data preprocessing. **Ki Yun Park, Satrajit Chakrabarty, Carl D. Hacker, Mikhail Milchenko, Aristeidis Sotiras, Daniel S. Marcus, Abraham Z. Snyder**: Methodology. **Ki Yun Park, Kara M. Donovan, Abraham Z. Snyder**: Visualization. **Joshua S. Shimony, Eric C. Leuthardt**: Funding acquisition. **Joshua S. Shimony, Eric C. Leuthardt, Abraham Z. Snyder**: Supervision. **Ki Yun Park, Joshua S. Shimony, Patrick H. Luckett, Aristeidis Sotiras, Eric C. Leuthardt, Abraham Z. Snyder** with contributions from all authors: Writing – review & editing.

## Declaration of Competing Interest

KYP, JSS, PHL, AZS, report the following conflict of interest. Licensing of Intellectual Property: Sora Neuroscience. AS reports the following conflict of interest. Stock ownership: TheraPanacea. DSM reports the following conflict of interest. Stock ownership: Sora Neuroscience, Flywheel Exchange LLC. ECL reports the following conflicts of interest. Stock ownership: Neurolutions, General Sensing, Osteovantage, Pear Therapeutics, Face to Face Biometrics, Immunovalent, Caeli Vascular, Acera, Sora Neuroscience, Inner Cosmos, Kinetrix, NeuroDev. Petal Surgical. Consultant: Monteris Medical, E15, Acera, Alcyone, Intellectual Ventures, Medtronic, Neurolutions, Osteovantage, Pear Therapeutics, Sante Ventures, Microbot. Licensing of Intellectual

Property: Neurolutions, Osteovantage, Caeli Vascular, Sora Neuroscience. Washington University owns equity in Neurolutions. The other authors report they have no competing interests.

## Data availability

Data will be made available on request.

## Acknowledgements

Parts of this work were funded by the Intellectual and Developmental Disabilities Research Center at Washington University award Number P50 HD103525.

### *Data and Code availability*

The OASIS3 dataset can be accessed publicly at https://www.oasis-brains.org/. Tumor data will be available upon request to ECL. The primary atlas registration pipeline used in this work is available at https://github.com/robbisg/4dfp_tools. ANTs registration used for non-linear registration can be found at http://stnava.github.io/ANTs/. Any other codes used in this study will be available upon request to KYP.

## Appendix A. Supporting information

Supplementary data associated with this article can be found in the online version at doi:10.1016/j.jneumeth.2023.110011.

## References

Alexander-Bloch, A., Lambiotte, R., Roberts, B., Giedd, J., Gogtay, N., Bullmore, E., 2012. The discovery of population differences in network community structure: New methods and applications to brain functional networks in schizophrenia. Neuroimage 59 (4), 3889–3900. ⟨https://www.sciencedirect.com/science/article/pii/S1053811911013164⟩.

Ashburner, J., 2007. A fast diffeomorphic image registration algorithm. Neuroimage 38 (1), 95–113. ⟨https://linkinghub.elsevier.com/retrieve/pii/S1053811907005848⟩.

Beckmann, C.F., DeLuca, M., Devlin, J.T., Smith, S.M., 2005. Investigations into resting-state connectivity using independent component analysis. Philos. Trans. R. Soc. Lond. B Biol. Sci. 360 (1457), 1001–1013. https://doi.org/10.1098/rstb.2005.1634.

Behzadi, Y., Restom, K., Liau, J., Liu, T.T., 2007. A component based noise correction method (CompCor) for BOLD and perfusion based fMRI. Neuroimage 37 (1), 90–101. https://doi.org/10.1016/j.neuroimage.2007.04.042.

Brett, M., Leff, A.P., Rorden, C., Ashburner, J., 2001. Spatial normalization of brain images with focal lesions using cost function masking. Neuroimage 14 (2), 486–500. https://doi.org/10.1006/nimg.2001.0845.

Bullmore, E., Sporns, O., 2009. Complex brain networks: graph theoretical analysis of structural and functional systems [2009 Nature Publishing Group]. Nat. Rev. Neurosci. 10 (3), 186–198. ⟨https://www.nature.com/articles/nrn2575⟩.

Chen, H.S.-M., Kumar, V.A., Johnson, J.M., Chen, M.M., Noll, K.R., Hou, P., Prabhu, S.S., Schomer, D.F., Liu, H.-L., 2021. Effect of brain normalization methods on the construction of functional connectomes from resting-state functional MRI in patients with gliomas. Magn. Reson Med 86 (1), 487–498. https://doi.org/10.1002/mrm.28690. ⟨https://onlinelibrary.wiley.com/doi/abs/⟩.

Craddock, R.C., James, G.A., Holtzheimer 3rd, P.E., Hu, X.P., Mayberg, H.S., 2012. A whole brain fMRI atlas generated via spatially constrained spectral clustering. Hum. Brain Mapp. 33 (8), 1914–1928. https://doi.org/10.1002/hbm.21333.

Crinion, J., Ashburner, J., Leff, A., Brett, M., Price, C., Friston, K., 2007. Spatial normalization of lesioned brains: performance evaluation and impact on fMRI analyses. Neuroimage 37 (3), 866–875. https://doi.org/10.1016/j.neuroimage.2007.04.065.

Daniel, A.G.S., Hacker, C.D., Lee, J.J., Dierker, D., Humphries, J.B., Shimony, J.S., Leuthardt, E.C., 2021. Homotopic functional connectivity disruptions in glioma patients are associated with tumor malignancy and overall survival. Neurooncol Adv. 3 (1), vdab176 https://doi.org/10.1093/noajnl/vdab176.

Dierker, D., Roland, J.L., Kamran, M., Rutlin, J., Hacker, C.D., Marcus, D.S., Milchenko, M., Miller-Thomas, M.M., Benzinger, T.L., Snyder, A.Z., Leuthardt, E.C., Shimony, J.S., 2017. Resting-state Functional Magnetic Resonance Imaging in Presurgical Functional Mapping: Sensorimotor Localization. Neuroimaging Clin. N. Am. 27 (4), 621–633. https://doi.org/10.1016/j.nic.2017.06.011.

Doucet, G., Naveau, M., Petit, L., Delcroix, N., Zago, L., Crivello, F., Jobard, G., Tzourio-Mazoyer, N., Mazoyer, B., Mellet, E., Joliot, M., 2011. Brain activity at rest: a multiscale hierarchical functional organization. J. Neurophysiol. 105 (6), 2753–2763. https://doi.org/10.1152/jn.00895.2010.

Eisinga, R., Heskes, T., Pelzer, B., Te Grotenhuis, M., 2017. Exact p-values for pairwise comparison of Friedman rank sums, with application to comparing classifiers. BMC Bioinforma. 18 (1), 68 https://doi.org/10.1186/s12859-017-1486-2.

Fan, L., Li, H., Zhuo, J., Zhang, Y., Wang, J., Chen, L., Yang, Z., Chu, C., Xie, S., Laird, A. R., Fox, P.T., Eickhoff, S.B., Yu, C., Jiang, T., 2016. The human brainnetome Atlas: a new brain atlas based on connectional architecture. Cereb. Cortex 26 (8), 3508–3526. https://doi.org/10.1093/cercor/bhw157.

Felleman, D., Van Essen, D., 1991. Distributed hierarchical processing in the primate cerebral cortex. Cereb. Cortex 1 (1). https://doi.org/10.1093/cercor/1.1.1.

Fonov, V.S., Evans, A.C., McKinstry, R.C., Almli, C.R., Collins, D.L., 2009. Unbiased nonlinear average age-appropriate brain templates from birth to adulthood. Neuroimage 47, S102.

Fox, M.D., Snyder, A.Z., Vincent, J.L., Corbetta, M., Van Essen, D.C., Raichle, M.E., 2005. The human brain is intrinsically organized into dynamic, anticorrelated functional networks. Proc. Natl. Acad. Sci. USA 102 (27), 9673–9678. https://doi.org/10.1073/pnas.0504136102.

Fox, M.D., Zhang, D., Snyder, A.Z., Raichle, M.E., 2009. The global signal and observed anticorrelated resting state brain networks. J. Neurophysiol. 101 (6), 3270–3283. https://doi.org/10.1152/jn.90777.2008.

Fox, M.E., King, T.Z., 2018. Functional connectivity in adult brain tumor patients: a systematic review. Brain Connect 8 (7), 381–397. https://doi.org/10.1089/brain.2018.0623.

Ghinda, D.C., Wu, J.S., Duncan, N.W., Northoff, G., 2018. How much is enough-Can resting state fMRI provide a demarcation for neurosurgical resection in glioma? Neurosci. Biobehav Rev. 84, 245–261. https://doi.org/10.1016/j.neubiorev.2017.11.019.

Gooya, A., Pohl, K.M., Bilello, M., Cirillo, L., Biros, G., Melhem, E.R., Davatzikos, C., 2012. GLISTR: glioma image segmentation and registration. IEEE Trans. Med Imaging 31 (10), 1941–1954. https://doi.org/10.1109/TMI.2012.2210558.

Gordon, E.M., Laumann, T.O., Adeyemo, B., Huckins, J.F., Kelley, W.M., Petersen, S.E., 2016. Generation and evaluation of a cortical area parcellation from resting-state correlations. Cereb. Cortex 26 (1), 288–303. https://doi.org/10.1093/cercor/bhu239.

Gordon, E.M., Laumann, T.O., Gilmore, A.W., Newbold, D.J., Greene, D.J., Berg, J.J., Ortega, M., Hoyt-Drazen, C., Gratton, C., Sun, H., Hampton, J.M., Coalson, R.S., Nguyen, A.L., McDermott, K.B., Shimony, J.S., Snyder, A.Z., Schlaggar, B.L., Petersen, S.E., Nelson, S.M., Dosenbach, N.U.F., 2017. Precision functional mapping of individual human brains. e797 Neuron 95 (4), 791–807. https://doi.org/10.1016/j.neuron.2017.07.011.

Gotts, S.J., Gilmore, A.W., Martin, A., 2020. Brain networks, dimensionality, and global signal averaging in resting-state fMRI: Hierarchical network structure results in low-dimensional spatiotemporal dynamics. Neuroimage 205, 116289. https://doi.org/10.1016/j.neuroimage.2019.116289.

Hacker, C.D., Laumann, T.O., Szrama, N.P., Baldassarre, A., Snyder, A.Z., Leuthardt, E.C., Corbetta, M., 2013. Resting state network estimation in individual subjects. Neuroimage 82, 616–633. https://doi.org/10.1016/j.neuroimage.2013.05.108.

Hallquist, M.N., Hillary, F.G., 2019. Graph theory approaches to functional network organization in brain disorders: A critique for a brave new small-world. Netw. Neurosci. 3 (1), 1–26. https://doi.org/10.1162/netn_a_00054.

Huntenburg, J.M., Bazin, P.L., Margulies, D.S., 2018. Large-scale gradients in human cortical organization. Trends Cogn. Sci. 22 (1), 21–31. https://doi.org/10.1016/j.tics.2017.11.002.

Isensee, F., Kickingereder, P., Wick, W., Bendszus, M., Maier-Hein, K.H., 2017. Brain tumor segmentation and radiomics survival prediction: Contribution to the brats 2017 challenge. Int. MICCAI Brainlesion Workshop 287–297.

Kaas, J.H., 1987. The organization of neocortex in mammals: implications for theories of brain function. Annu. Rev. Psychol. 38 (1), 129–151.

LaMontagne, P.J., Benzinger, T.L.S., Morris, J.C., Keefe, S., Hornbeck, R., Xiong, C., Grant, E., Hassenstab, J., Moulder, K., Vlassenko, A.G., Raichle, M.E., Cruchaga, C., Marcus, D., 2019. OASIS-3: longitudinal neuroimaging, clinical, and cognitive dataset for normal aging and Alzheimer disease. medRxiv. https://doi.org/10.1101/2019.12.13.19014902.

Lee, M.H., Hacker, C.D., Snyder, A.Z., Corbetta, M., Zhang, D., Leuthardt, E.C., Shimony, J.S., 2012. Clustering of resting state networks. PLoS One 7 (7), e40370. https://doi.org/10.1371/journal.pone.0040370.

Leuthardt, E.C., Guzman, G., Bandt, S.K., Hacker, C., Vellimana, A.K., Limbrick, D., Milchenko, M., Lamontagne, P., Speidel, B., Roland, J., Miller-Thomas, M., Snyder, A.Z., Marcus, D., Shimony, J., Benzinger, T.L.S., 2018. Integration of resting state functional MRI into clinical practice - A large single institution experience. PLoS One 13 (6), e0198349. https://doi.org/10.1371/journal.pone.0198349.

Lv, K., Cao, X., Wang, R., Du, P., Fu, J., Geng, D., Zhang, J., 2022. Neuroplasticity of glioma patients: brain structure and topological network. Front Neurol. 13, 871613 https://doi.org/10.3389/fneur.2022.871613.

Nemenyi, P. (1963). Confidence Intervals and Confidence Boxes Corresponding to Some Quick and Easy Tests. Biometrics, 19(4), 655-&. <Go to ISI>://WOS:A19637265A00034.

Newman, M.E.J., 2004. Fast algorithm for detecting community structure in networks. Phys. Rev. E 69 (6), 066133 https://link.aps.org/doi/10.1103/PhysRevE.69.066133.

Ou, Y., Sotiras, A., Paragios, N., Davatzikos, C., 2011. DRAMMS: deformable registration via attribute matching and mutual-saliency weighting. Med. Image Anal. 15 (4), 622–639. ⟨https://www.ncbi.nlm.nih.gov/pmc/articles/PMC3012150/⟩.

Park, K.Y., Lee, J.J., Dierker, D., Marple, L.M., Hacker, C.D., Roland, J.L., Marcus, D.S., Milchenko, M., Miller-Thomas, M.M., Benzinger, T.L., Shimony, J.S., Snyder, A.Z., Leuthardt, E.C., 2020. Mapping language function with task-based vs. resting-state functional MRI. PLoS One 15 (7), e0236423. https://doi.org/10.1371/journal.pone.0236423.

Power, J.D., Cohen, A.L., Nelson, S.M., Wig, G.S., Barnes, K.A., Church, J.A., Vogel, A.C., Laumann, T.O., Miezin, F.M., Schlaggar, B.L., Petersen, S.E., 2011. Functional

network organization of the human brain. Neuron 72 (4), 665–678. https://doi.org/10.1016/j.neuron.2011.09.006.

Power, J.D., Barnes, K.A., Snyder, A.Z., Schlaggar, B.L., Petersen, S.E., 2012. Spurious but systematic correlations in functional connectivity MRI networks arise from subject motion. Neuroimage 59 (3), 2142–2154. https://doi.org/10.1016/j.neuroimage.2011.10.018.

Power, J.D., Lynch, C.J., Silver, B.M., Dubin, M.J., Martin, A., Jones, R.M., 2019. Distinctions among real and apparent respiratory motions in human fMRI data. Neuroimage 201, 116041. https://doi.org/10.1016/j.neuroimage.2019.116041.

Rayshubskiy, A., Wojtasiewicz, T.J., Mikell, C.B., Bouchard, M.B., Timerman, D., Youngerman, B.E., McGovern, R.A., Otten, M.L., Canoll, P., McKhann 2nd, G.M., Hillman, E.M., 2014. Direct, intraoperative observation of ~0.1 Hz hemodynamic oscillations in awake human cortex: implications for fMRI. Neuroimage 87, 323–331. https://doi.org/10.1016/j.neuroimage.2013.10.044.

Ripolles, P., Marco-Pallares, J., de Diego-Balaguer, R., Miro, J., Falip, M., Juncadella, M., Rubio, F., Rodriguez-Fornells, A., 2012. Analysis of automated methods for spatial normalization of lesioned brains. Neuroimage 60 (2), 1296–1306. https://doi.org/10.1016/j.neuroimage.2012.01.094.

Rubinov, M., & Sporns, O. (2010). Complex network measures of brain connectivity: Uses and interpretations. *Neuroimage*, *52*(3), 1059–1069. ⟨https://www.sciencedirect.com/science/article/pii/S105381190901074X⟩ (Computational Models of the Brain).

Schaefer, A., Kong, R., Gordon, E.M., Laumann, T.O., Zuo, X.N., Holmes, A.J., Eickhoff, S. B., Yeo, B.T.T., 2018. Local-global parcellation of the human cerebral cortex from intrinsic functional connectivity MRI. Cereb. Cortex 28 (9), 3095–3114. https://doi.org/10.1093/cercor/bhx179.

Seeley, W.W., Menon, V., Schatzberg, A.F., Keller, J., Glover, G.H., Kenna, H., Reiss, A.L., Greicius, M.D., 2007. Dissociable intrinsic connectivity networks for salience processing and executive control. J. Neurosci. 27 (9), 2349–2356. https://doi.org/10.1523/JNEUROSCI.5587-06.2007.

Shen, X., Tokoglu, F., Papademetris, X., Constable, R.T., 2013. Groupwise whole-brain parcellation from resting-state fMRI data for network node identification. Neuroimage 82, 403–415. https://doi.org/10.1016/j.neuroimage.2013.05.081.

Shulman, G.L., Pope, D.L., Astafiev, S.V., McAvoy, M.P., Snyder, A.Z., Corbetta, M., 2010. Right hemisphere dominance during spatial selective attention and target detection occurs outside the dorsal frontoparietal network. J. Neurosci. 30 (10), 3640–3651. https://doi.org/10.1523/JNEUROSCI.4085-09.2010.

Sighinolfi, G., Mitolo, M., Testa, C., Martinoni, M., Evangelisti, S., Rochat, M.J., Zoli, M., Mazzatenta, D., Lodi, R., Tonon, C., 2022. What Can Resting-State fMRI Data Analysis Explain about the Functional Brain Connectivity in Glioma Patients? Tomography 8 (1), 267–280. https://doi.org/10.3390/tomography8010021.

Smyser, C.D., Inder, T.E., Shimony, J.S., Hill, J.E., Degnan, A.J., Snyder, A.Z., & Neil, J.J. (2010). Longitudinal analysis of neural network development in preterm infants [Research Support, N.I.H., Extramural Research Support, Non-U.S. Gov't]. Cereb Cortex, 20(12), 2852–2862. https://doi.org/10.1093/cercor/bhq035.

Tzourio-Mazoyer, N., Landeau, B., Papathanassiou, D., Crivello, F., Etard, O., Delcroix, N., Mazoyer, B., Joliot, M., 2002. Automated Anatomical Labeling of Activations in SPM Using a Macroscopic Anatomical Parcellation of the MNI MRI Single-Subject Brain. Neuroimage 15 (1), 273–289. ⟨https://www.sciencedirect.com/science/article/pii/S1053811901909784⟩.

Ulmer, J.L., Krouwer, H.G., Mueller, W.M., Ugurel, M.S., Kocak, M., Mark, L.P., 2003. Pseudo-reorganization of language cortical function at fMR imaging: a consequence of tumor-induced neurovascular uncoupling. AJNR Am. J. Neuroradiol. 24 (2), 213–217. ⟨https://www.ncbi.nlm.nih.gov/pubmed/12591636⟩.

Wang, Z., Bovik, A.C., Sheikh, H.R., Simoncelli, E.P., 2004. Image quality assessment: from error visibility to structural similarity. IEEE Trans. Image Process. 13 (4), 600–612.

Yeo, B.T., Krienen, F.M., Sepulcre, J., Sabuncu, M.R., Lashkari, D., Hollinshead, M., Roffman, J.L., Smoller, J.W., Zollei, L., Polimeni, J.R., Fischl, B., Liu, H., Buckner, R. L., 2011. The organization of the human cerebral cortex estimated by intrinsic functional connectivity. J. Neurophysiol. 106 (3), 1125–1165. https://doi.org/10.1152/jn.00338.2011.

Zang, Y.-F., He, Y., Zhu, C.-Z., Cao, Q.-J., Sui, M.-Q., Liang, M., Tian, L.-X., Jiang, T.-Z., Wang, Y.-F., 2007. Altered baseline brain activity in children with ADHD revealed by resting-state functional MRI. Brain Dev. 29 (2), 83–91.

Zou, Q.-H., Zhu, C.-Z., Yang, Y., Zuo, X.-N., Long, X.-Y., Cao, Q.-J., Wang, Y.-F., Zang, Y.-F., 2008. An improved approach to detection of amplitude of low-frequency fluctuation (ALFF) for resting-state fMRI: Fractional ALFF. J. Neurosci. Methods 172 (1), 137–141. ⟨https://www.sciencedirect.com/science/article/pii/S0165027008002458⟩.